

A REDUCED BASIS ELEMENT METHOD FOR THE STEADY STOKES PROBLEM

ALF EMIL LØVGREN¹, YVON MADAY² AND EINAR M. RØNQUIST³

Abstract. The reduced basis element method is a new approach for approximating the solution of problems described by partial differential equations. The method takes its roots in domain decomposition methods and reduced basis discretizations. The basic idea is to first decompose the computational domain into a series of subdomains that are deformations of a few reference domains (or generic computational parts). Associated with each reference domain are precomputed solutions corresponding to the same governing partial differential equation, but solved for different choices of deformations of the reference subdomains and mapped onto the reference shape. The approximation corresponding to a new shape is then taken to be a linear combination of the precomputed solutions, mapped from the generic computational part to the actual computational part. We extend earlier work in this direction to solve incompressible fluid flow problems governed by the steady Stokes equations. Particular focus is given to satisfying the inf-sup condition, to *a posteriori* error estimation, and to “gluing” the local solutions together in the multidomain case.

1991 Mathematics Subject Classification. 65C20, 93A30, 65N30, 65N35, 65N15, 76D07.

The dates will be set by the publisher.

1. INTRODUCTION

The reduced basis element method is a new approach for approximating the solution of problems described by partial differential equations. The method takes its roots in domain decomposition methods and in reduced basis discretizations.

Reduced basis methods have been introduced in [8] and [15] as a computational approach that makes it possible to obtain a good approximation by solving very small systems. The problem is described by partial differential equations, and the solution depends on one or more parameters. For many problems, the dependency of the solution on the parameters is often regular. It is thus possible to approximate the solution for general values of the parameters as a linear combination of precomputed solutions for certain instances (or “snapshots”) of the parameters. The best linear combination is often found by a Galerkin procedure.

The reduced basis framework may be applied to a particular region in physical space. The parameters may be material properties or geometric parameters, say. An extension of this framework to solve more complex

Keywords and phrases: Stokes flow, reduced basis, reduced order model, domain decomposition, mortar method, output bounds, a posteriori error estimators

¹ Norwegian University of Science and Technology, Department of Mathematical Sciences

² Laboratoire Jacques-Louis Lions, Université Pierre et Marie Curie

³ Norwegian University of Science and Technology, Department of Mathematical Sciences, email: ronquist@math.ntnu.no, fax: +47 73 59 35 24, phone: +47 73 59 35 47, address: N-7491 Trondheim, Norway

problems is based on first decomposing the domain into generic building blocks, and then applying the reduced basis approach locally in the context of each building block. A global approximation is then constructed by gluing together the local approximations using a mortar type method. These are the essential ingredients of the reduced basis element method. The term "element" here refers to the notion of a generic building block or part like in the spectral element or mortar element method.

The reduced basis element method was introduced in [13] in the context of solving the Laplace equation in a deformed geometry. In that work, the computational domain was broken into generic building blocks or parts (e.g., "pipes"), and the geometry of each part played the role of the parameters. The reduced basis approximations associated with all the parts were glued together through the use of Lagrange multipliers.

Further progress was made in [14] in the context of solving a thermal fin problem. In particular, *a posteriori* error bounds were developed for the output of interest. We remark that this aspect represents an essential ingredient in developing practical reduced basis methods. Since it is *a priori* difficult to guess the number of reduced elements required in practical computations, *a posteriori* error bounds represent practical tools which allow us to certify the computational results.

In this paper, we extend the results in [13] to solve incompressible fluid flow problems modeled by the steady Stokes equations. What is similar to earlier work is the construction of a reduced basis for a particular generic part based on "geometric snapshots," and the representation of the individual basis functions on a reference domain associated with the generic part. However, there are also several new extensions and new aspects considered in this paper.

In Section 2 we state the steady Stokes problem we are considering together with the particular geometries we are dealing with. The spectral discretization used to construct the reduced basis is also briefly reviewed. In Section 3 we introduce the reduced basis method in the single domain case, and present numerical results. Two different methods are presented, one where the velocity-pressure pair is computed (Method 1), and one where only the velocity is computed (Method 2). We also extend the *a posteriori* analysis in [16] and [18] to the compliant case.

Finally, in Section 4, we turn our attention to the multiple domain case. Of particular interest is the proper gluing of the local approximations. As in the earlier work, we use a mortar type method based on Lagrange multipliers; see [4]. The pressure is only in L^2 , so no particular problems occur here. However, special care has to be given to the definition of the Lagrange multiplier spaces associated with the velocity vectorial field.

2. THE STEADY STOKES PROBLEM

2.1. Governing equations

We consider here the two-dimensional steady Stokes equations

$$\begin{aligned} -\nu\Delta\mathbf{u} + \nabla p &= \mathbf{f} & \text{in } \Omega, \\ \nabla \cdot \mathbf{u} &= 0 & \text{in } \Omega, \end{aligned} \tag{2.1}$$

where $\mathbf{u} = (u_1, u_2)$ is the velocity field, p is the pressure, $\mathbf{f} = (f_1, f_2)$ is a prescribed volumetric body force, and ν is the fluid viscosity; see [1]. The steady Stokes equations model laminar flow at very low Reynolds number; the nonlinear advection term of the Navier-Stokes equations is neglected, and we are left with a linear problem. The velocity formulation (2.1) is an appropriate model when ν is constant and for certain types of boundary conditions. For all the problems studied in this paper, this model will suffice. For more general problems, the full stress formulation of the steady Stokes equations should be used.

We consider here a domain Ω with an inflow boundary, Γ_{in} , an outflow boundary, Γ_{out} , and wall boundaries, Γ_w . On this domain we introduce the velocity space

$$X = \{\mathbf{v} \in (H^1(\Omega))^2, \quad \mathbf{v}|_{\Gamma_w} = 0 \text{ and } v_t|_{\Gamma_{in}} = v_t|_{\Gamma_{out}} = 0\}, \tag{2.2}$$

where v_t is the tangential velocity component. In addition, we have the Neumann type boundary conditions given by specifying $\sigma_n = \nu \frac{\partial u_n}{\partial n} - p$ to be $\sigma_n^{in} = -1$ along Γ_{in} and $\sigma_n^{out} = 0$ along Γ_{out} ; here, u_n is the normal velocity component and $\partial/\partial n$ denotes the derivative in the outward normal direction. From the divergence free condition and the fact that $u_t = 0$ along the inflow and outflow boundaries, we deduce that $\frac{\partial u_n}{\partial n} = 0$ along Γ_{in} and Γ_{out} , which implies that the Neumann conditions correspond to specifying the pressure along the inflow and outflow boundaries (in a weak sense).

With the given boundary conditions, we define the pressure space to be

$$M = L^2(\Omega). \quad (2.3)$$

In order to solve the steady Stokes equations we define the bilinear forms

$$a(\mathbf{v}, \mathbf{w}) = \nu \int_{\Omega} \nabla \mathbf{v} \cdot \nabla \mathbf{w} \, d\Omega = \nu \sum_{i,j=1}^2 \int_{\Omega} \frac{\partial v_i}{\partial x_j} \frac{\partial w_i}{\partial x_j} \, d\Omega, \quad (2.4)$$

$$b(\mathbf{v}, q) = - \int_{\Omega} q \nabla \cdot \mathbf{v} \, d\Omega = \sum_{i=1}^2 - \int_{\Omega} q \frac{\partial v_i}{\partial x_i} \, d\Omega, \quad (2.5)$$

and consider the weak form: Find $\mathbf{u} \in X$ and $p \in M$ such that

$$\begin{aligned} a(\mathbf{u}, \mathbf{v}) + b(\mathbf{v}, p) &= l(\mathbf{v}) \quad \forall \mathbf{v} \in X \\ b(\mathbf{u}, q) &= 0 \quad \forall q \in M, \end{aligned} \quad (2.6)$$

where

$$l(\mathbf{v}) = (\mathbf{f}, \mathbf{v}) + \int_{\Gamma_{in}} \sigma_n^{in} \mathbf{v} \cdot \mathbf{n} \, ds + \int_{\Gamma_{out}} \sigma_n^{out} \mathbf{v} \cdot \mathbf{n} \, ds. \quad (2.7)$$

For the steady Stokes problem (2.6), the coercivity condition

$$a(\mathbf{w}, \mathbf{w}) \geq \alpha \|\mathbf{w}\|_{H^1(\Omega)}^2, \quad \forall \mathbf{w} \in X, \quad \alpha > 0, \quad (2.8)$$

and the inf-sup condition

$$\inf_{q \in M} \sup_{\mathbf{v} \in X} \frac{b(\mathbf{v}, q)}{\|q\|_{L^2(\Omega)} \|\mathbf{v}\|_{H^1(\Omega)}} = \beta > 0, \quad (2.9)$$

see [2] and [6], are both satisfied, which ensures a unique solution.

2.2. Mapping to a reference domain

In the following, we focus on two-dimensional problems where the domain Ω is at least Lipschitz continuous, and can be considered as a mapping of a reference domain $\hat{\Omega} = (-1, 1)^2$, see Figure 1. We write $\Omega = \Phi(\hat{\Omega})$, where Φ is a one-to-one mapping, and the left and right vertical edges on $\hat{\Omega}$ correspond to the inflow and outflow boundaries on Ω , respectively. In terms of the reference variables, we can then alternatively express (2.4) and (2.5) as

$$a(\mathbf{v}, \mathbf{w}) = \nu \int_{\hat{\Omega}} \mathcal{J}^{-T} \hat{\nabla}(\mathbf{v} \circ \Phi) \cdot \mathcal{J}^{-T} \hat{\nabla}(\mathbf{w} \circ \Phi) |J| \, d\hat{\Omega}, \quad (2.10)$$

$$b(\mathbf{v}, q) = - \int_{\hat{\Omega}} (q \circ \Phi) \hat{\nabla} \cdot [\mathcal{J}^{-1}(\mathbf{v} \circ \Phi)] |J| \, d\hat{\Omega}, \quad (2.11)$$

where \mathcal{J} is the Jacobian of Φ ,

$$\mathcal{J} = \begin{bmatrix} \frac{\partial x}{\partial \xi} & \frac{\partial x}{\partial \eta} \\ \frac{\partial y}{\partial \xi} & \frac{\partial y}{\partial \eta} \end{bmatrix}, \quad (2.12)$$

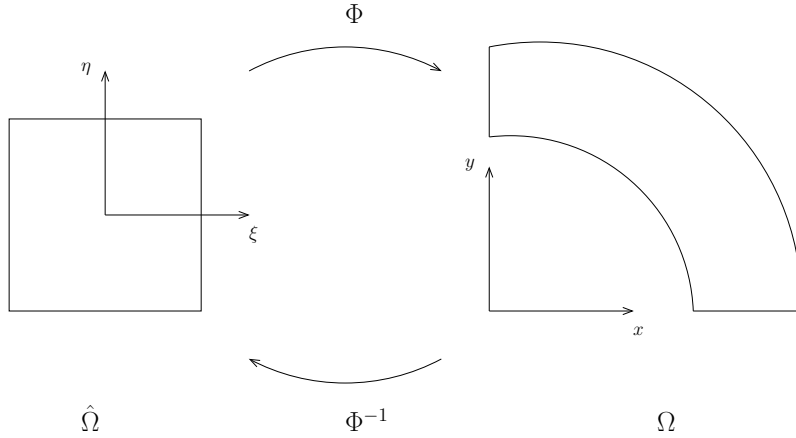


FIGURE 1. Mapping of the reference domain.

and J denotes the determinant of \mathcal{J} . A similar transformation can be done to the linear form (2.7); in the following, we set $\mathbf{f} = \mathbf{0}$ and $\nu = 1$.

As is well known, this transformation is useful for the discretization of the Stokes problem. However, it will also prove very useful when we consider the reduced basis element method. As discussed in Section 3, we will exploit the fact that the solution \mathbf{u} and p can be considered dependent on the geometry (or shape) through the mapping Φ , i.e., $\mathbf{u} = \mathbf{u}(\Phi)$ and $p = p(\Phi)$; see [13].

2.3. Spectral discretization

We now consider a discretization of the steady Stokes problem (2.6) using a pure spectral method based on high order polynomials; see [11] and [12]. For the sake of completeness and in order to introduce the proper notation, let us first briefly recall some classical material on spectral approximation for Stokes flows. Let $\mathbb{P}_n(\hat{\Omega})$ be the space of all functions which are polynomials of degree less than or equal to n in each spatial direction of the reference domain $\hat{\Omega}$. The discrete space for the velocity is then taken to be

$$X_{\mathcal{N}} = \{\mathbf{v} \in X, \quad \mathbf{v} \circ \Phi \in (\mathbb{P}_{\mathcal{N}}(\hat{\Omega}))^2\}, \quad (2.13)$$

while the discrete space for the pressure is

$$M_{\mathcal{N}} = \{q \in M, \quad q \circ \Phi \in \mathbb{P}_{\mathcal{N}-2}(\hat{\Omega})\}. \quad (2.14)$$

The bases for $X_{\mathcal{N}}$ and $M_{\mathcal{N}}$ are conveniently expressed in terms of the reference variables ξ and η . As a basis for $X_{\mathcal{N}}$ we use a nodal basis through the tensor-product Gauss-Lobatto Legendre (GLL) points, while the basis for $M_{\mathcal{N}}$ is a nodal basis through the tensor-product Gauss-Legendre (GL) points; see [11] and [12]. Specifically, we write $\mathbf{u}_{\mathcal{N}} \in X_{\mathcal{N}}$ as

$$(\mathbf{u}_{\mathcal{N}} \circ \Phi)(\xi, \eta) = \sum_{i,j=0}^{\mathcal{N}} \mathbf{u}_{ij} \ell_i(\xi) \ell_j(\eta), \quad (2.15)$$

where $\ell_i(\xi)$ refers to a one-dimensional \mathcal{N} -th order Lagrangian interpolant through the GLL points ξ_m , $m = 0, \dots, \mathcal{N}$; hence, $\ell_i(\xi_m) \ell_j(\xi_n) = \delta_{im} \delta_{jn}$ for a given point (ξ_m, ξ_n) in the underlying tensor-product GLL grid.

In a similar fashion, we write $p_{\mathcal{N}} \in M_{\mathcal{N}}$ as

$$(p_{\mathcal{N}} \circ \Phi)(\xi, \eta) = \sum_{i,j=0}^{\mathcal{N}-2} p_{ij} \tilde{\ell}_i(\xi) \tilde{\ell}_j(\eta), \quad (2.16)$$

where $\tilde{\ell}_i(\xi)$ refers to a one-dimensional $(\mathcal{N}-2)$ -th order Lagrangian interpolant through the (interior) GL points ζ_m , $m = 0, \dots, \mathcal{N}-2$; hence, $\tilde{\ell}_i(\zeta_m) \tilde{\ell}_j(\zeta_n) = \delta_{im} \delta_{jn}$ for a given point in the tensor-product GL grid.

The discrete velocity $\mathbf{u}_{\mathcal{N}} \in X_{\mathcal{N}}$ is then uniquely determined by $(\mathcal{N}+1)^2$ coefficients for each spatial component, where some of the coefficients are fixed due to the prescribed Dirichlet boundary conditions. The discrete pressure is determined by $(\mathcal{N}-1)^2$ basis coefficients.

The mapping Φ is realized computationally through a Gordon-Hall algorithm, see [9], and by using an isoparametric representation of the geometry. Each edge of Ω is given as a one-to-one mapping of a corresponding edge $[-1, 1]$ on $\hat{\Omega}$ and approximated as an \mathcal{N} -th order polynomial; the location of the interior points are then simply $(x_m, y_n) = \Phi(\xi_m, \xi_n)$, $1 \leq m, n \leq \mathcal{N}-1$.

The bilinear forms and the linear form in (2.6) are expressed in terms of the reference variables, and the integrals are evaluated using GLL and GL quadrature. This gives us the following discrete system: Find $\mathbf{u}_{\mathcal{N}} \in X_{\mathcal{N}}$ and $p_{\mathcal{N}} \in M_{\mathcal{N}}$ such that

$$\begin{aligned} a_{\mathcal{N}}(\mathbf{u}_{\mathcal{N}}, \mathbf{v}) + b_{\mathcal{N}}(\mathbf{v}, p_{\mathcal{N}}) &= l_{\mathcal{N}}(\mathbf{v}) \quad \forall \mathbf{v} \in X_{\mathcal{N}} \\ b_{\mathcal{N}}(\mathbf{u}_{\mathcal{N}}, q) &= 0 \quad \forall q \in M_{\mathcal{N}}, \end{aligned} \quad (2.17)$$

where $a_{\mathcal{N}}$, $b_{\mathcal{N}}$ and $l_{\mathcal{N}}$ refer to integration of the bilinear and linear forms using Gauss-type quadrature. Using the chosen bases (2.15) and (2.16), we arrive at a system of algebraic equations for the unknown basis coefficients; this system is solved using the conjugate gradient method in the context of the Uzawa algorithm; see [12].

We remark that the use of a spectral approximation is legitimate here since the solution of the Stokes problem with the prescribed boundary conditions and the selected geometries is rather regular (especially in weighted norms [5]) and very rapid convergence is expected. For any solution to the Stokes problem we consider in the following, we assume that

$$\varepsilon_{\mathcal{N}} \equiv \|\mathbf{u} - \mathbf{u}_{\mathcal{N}}\|_{H^1} \quad (2.18)$$

is much smaller than the tolerance we want to obtain for the computational results based on the methods we now discuss.

3. A REDUCED BASIS METHOD

3.1. Geometry as a parameter

In Section 2 we considered the numerical solution of a steady Stokes problem using a pure spectral method based on high order polynomials. We had given a domain Ω as well as prescribed boundary conditions along $\partial\Omega$.

Imagine now that we would like to solve similar problems, i.e., the same governing equations, imposing the same boundary conditions, but now in a different domain. The only restriction is that the new domain should also be obtained as the deformation of the reference domain $\hat{\Omega}$ through some regular one-to-one mapping; see Figure 1.

The mapping from Ω onto the reference domain as explained in Section 2.2, suggests that the solution of the steady Stokes problem will depend on the geometry (or shape) of the domain in a fairly regular manner. The idea behind the reduced basis method is to exploit this fact. We will first solve the steady Stokes problem for different “snapshots” of possible shapes, and then express the solution corresponding to a new and untried shape as a linear combination of the precomputed solutions. To find the best linear combination, a Galerkin procedure will be used.

Note that the standard velocity and pressure bases introduced in Section 2.3 are expressed in terms of the reference variables. In the reduced basis method, we will also express the bases with reference to $\hat{\Omega}$, but now the basis functions will be the precomputed steady Stokes solutions mapped to the reference domain $\hat{\Omega}$.

3.2. Precomputing the basis solutions

We propose to use the same technique as for the Poisson problem in [13], in order to generate basis functions for the steady Stokes problem. For a sample set of mappings of a reference domain, $\{\Phi_i : \hat{\Omega} \rightarrow \Omega_i\}_{i=1}^N$, the steady Stokes problem (2.1) with exact solutions (\mathbf{u}^i, p^i) are approximated by the numerical solutions of (2.17) which we denote by $(\mathbf{u}_i \equiv \mathbf{u}_{\mathcal{N}}^i, p_i \equiv p_{\mathcal{N}}^i)$. Again the left and right edges of $\hat{\Omega}$ correspond to the inflow and outflow boundaries on Ω_i , respectively. These solutions are then used as basis functions to find the solution for a generic deformation. In order to do this we must map the solutions found on the deformed geometries,

$$\{(\mathbf{u}_i, p_i) \in X_{\mathcal{N}}(\Omega_i) \times M_{\mathcal{N}}(\Omega_i)\}_{i=1}^N, \quad (3.1)$$

to the reference domain, where they are stored. The pressure is a scalar field and will be mapped as such, $\hat{p}_i(\xi, \eta) = p_i \circ \Phi_i(\xi, \eta)$. Since the regular mapping $\Phi_i(\xi, \eta) = (x, y)$ is one-to-one from $\hat{\Omega}$ to Ω_i , this is well defined. The velocity solution, \mathbf{u}_i , is a divergence free vector field on the deformed domain, and we want the solution to keep this property when mapped to the reference domain. In particular, this means that if the flow is perpendicular to a surface of the deformed domain, the mapped flow should be perpendicular to the mapped surface. If we let $\hat{\nabla}$ be the gradient operator on the reference domain, we have the following relationship with the gradient operator on the deformed domain

$$\hat{\nabla} = \mathcal{J}_i^T \nabla. \quad (3.2)$$

To find the proper mapping for the velocity, we start with the fact that

$$\int_{\Omega_i} q \nabla \cdot \mathbf{u}_i \, d\Omega_i = 0 \quad \forall q \in M_{\mathcal{N}}(\Omega_i), \quad (3.3)$$

and demand that $\hat{\mathbf{u}}_i = \Psi_i(\mathbf{u}_i)$ satisfies

$$\int_{\hat{\Omega}} \hat{q} \hat{\nabla} \cdot \hat{\mathbf{u}}_i \, d\hat{\Omega} = 0 \quad \forall \hat{q} \in M_{\mathcal{N}}(\hat{\Omega}). \quad (3.4)$$

By mapping the integral in (3.4) to Ω_i , we get

$$\int_{\Omega_i} q \nabla \cdot [\mathcal{J}_i(\hat{\mathbf{u}}_i \circ \Phi_i^{-1})|J_i^{-1}|] \, d\Omega_i = 0 \quad \forall q \in M_{\mathcal{N}}(\Omega_i). \quad (3.5)$$

Equation (3.5) holds if $\mathcal{J}_i(\hat{\mathbf{u}}_i \circ \Phi_i^{-1})|J_i^{-1}| = \mathbf{u}_i$, which is known as Piola's transformation; see [17] and [7] for general properties. The proper mapping of the velocity from Ω_i to $\hat{\Omega}$ will therefore be

$$\hat{\mathbf{u}}_i = \Psi_i(\mathbf{u}_i) = \mathcal{J}_i^{-1}(\mathbf{u}_i \circ \Phi_i)|J_i|, \quad (3.6)$$

where

$$\mathcal{J}_i^{-1} = \begin{bmatrix} \frac{\partial \xi}{\partial x} & \frac{\partial \xi}{\partial y} \\ \frac{\partial \eta}{\partial x} & \frac{\partial \eta}{\partial y} \end{bmatrix} = \frac{1}{J} \begin{bmatrix} \frac{\partial y}{\partial \eta} & -\frac{\partial x}{\partial \eta} \\ -\frac{\partial y}{\partial \xi} & \frac{\partial x}{\partial \xi} \end{bmatrix}. \quad (3.7)$$

Mapping the velocity-vectors to the reference domain in this way, will certainly keep the velocity perpendicular to the same lines on the reference domain as the lines' mapped counterparts on the deformed domain, and the

velocity will be divergence free on the reference domain. We define the reduced basis reference spaces as

$$\begin{aligned}\hat{V}_N = V_N(\hat{\Omega}) &= \text{span}\{\hat{\mathbf{u}}_i, \quad i = 1, \dots, N\}, \\ \hat{M}_N = M_N(\hat{\Omega}) &= \text{span}\{\hat{p}_i, \quad i = 1, \dots, N\}.\end{aligned}\tag{3.8}$$

Note here that the basis functions $\hat{\mathbf{u}}_i$ are divergence free (thus the standard notation "V" for the associated space), but unfortunately the basis functions are not polynomials in $(\mathbb{P}_N(\hat{\Omega}))^2$. Rather, due to our choice of an isoparametric representation of the geometry, the basis functions $\hat{\mathbf{u}}_i$ are polynomials in $(\mathbb{P}_{2N}(\hat{\Omega}))^2$.

Some of the precomputed basis functions are not symmetric with respect to the horizontal center-line $\eta = 0$ in the reference domain. These basis functions are reflected across the line $\eta = 0$ in order to enrich the basis and to eliminate directional effects; see [13]. In the following, we let N denote the total number of basis functions such that the definition of the reduced basis reference spaces in (3.8) still holds.

For a generic domain $\Omega = \Phi(\hat{\Omega})$ we will now define the reduced basis solution spaces $X_N \subset X_{\mathcal{N}}$ and $M_N \subset M_{\mathcal{N}}$ that we will use. Our objective is to find a unique reduced basis solution $\mathbf{u}_N \in X_N$ and $p_N \in M_N$ satisfying

$$\begin{aligned}a_N(\mathbf{u}_N, \mathbf{v}) + b_N(\mathbf{v}, p_N) &= l_N(\mathbf{v}) \quad \forall \mathbf{v} \in X_N \\ b_N(\mathbf{u}_N, q) &= 0 \quad \forall q \in M_N.\end{aligned}\tag{3.9}$$

As before the coercivity of $a(\cdot, \cdot)$ holds for all $\mathbf{v} \in X_N$. The inf-sup condition (2.9), however, depends strongly on X_N and M_N .

Since we have assumed that $\Phi : \hat{\Omega} \rightarrow \Omega$ is one-to-one, and the pressure p_N is a scalar field over Ω , we define the reduced basis pressure space M_N as

$$M_N = \text{span}\{\hat{p}_i \circ \Phi^{-1}, \quad i = 1, \dots, N\}.\tag{3.10}$$

We could map the precomputed velocity fields $\hat{\mathbf{u}}_i$ to the new geometry Ω as

$$\Psi^{-1}(\hat{\mathbf{u}}_i) \equiv \mathcal{J}(\hat{\mathbf{u}}_i \circ \Phi^{-1})|J^{-1}|, \quad i = 1, \dots, N,\tag{3.11}$$

and then define the discrete velocity space X_N^0 as equal to the space

$$V_N = \text{span}\{\Psi^{-1}(\hat{\mathbf{u}}_i), \quad i = 1, \dots, N\}.\tag{3.12}$$

Unfortunately, due to the inverse Piola transform (3.11), the complexity of the functions $\Psi^{-1}(\hat{\mathbf{u}}_i)$ has increased even more in the sense that they are not even polynomials. We thus set

$$X_N^0 = \text{span}\{\tilde{\mathbf{u}}_i = \mathcal{I}_N(\Psi^{-1}(\hat{\mathbf{u}}_i) \circ \Phi) \circ \Phi^{-1}, \quad i = 1, \dots, N\}.\tag{3.13}$$

where \mathcal{I}_N is the interpolation operator defined over $\mathcal{C}^0(\hat{\Omega})$ at the Gauss-Lobatto Legendre points (ξ_m, ξ_n) , $0 \leq m, n \leq N$ onto $\mathbb{P}_N(\hat{\Omega})$. By construction, X_N^0 is now a subspace of $X_{\mathcal{N}}$, but the basis functions for X_N^0 are now only approximately divergence free. Specifically, using the optimality of the interpolation operator both in the L^2 and H^1 norms together with the fact that $\text{div}(\Psi^{-1}\Psi_i(\mathbf{u}^i)) = 0$ in Ω , it can be proven that

$$\|\nabla \cdot \tilde{\mathbf{u}}_i\|_{L^2(\Omega)} \sim \mathcal{O}(\varepsilon_N).\tag{3.14}$$

We now present two different methods to solve the steady Stokes problem (3.9).

3.3. Method 1

In our first method for choosing the reduced basis velocity space we will define X_N such that (3.9) can be solved directly for both the velocity and the pressure. In order to properly satisfy the inf-sup condition we

have to enrich the velocity basis. One way of doing this is for each pressure solution \hat{p}_i that spans \hat{M}_N , to find $\hat{\mathbf{v}}(\hat{p}_i) = \hat{\mathbf{v}}_i \in \hat{X}_N = X_N(\hat{\Omega})$ such that

$$\hat{\mathbf{v}}_i = \arg \max_{\hat{\mathbf{u}} \in \hat{X}_N} \frac{\int_{\hat{\Omega}} \hat{p}_i \hat{\nabla} \cdot \hat{\mathbf{u}} d\hat{\Omega}}{\|\hat{\mathbf{u}}\|_{H^1}}. \quad (3.15)$$

It is well known that the solution of (3.15) also satisfies

$$\int_{\hat{\Omega}} \hat{\nabla} \hat{\mathbf{v}}_i \cdot \hat{\nabla} \hat{\mathbf{w}} d\hat{\Omega} = \int_{\hat{\Omega}} \hat{p}_i \hat{\nabla} \cdot \hat{\mathbf{w}} d\hat{\Omega}, \quad \forall \hat{\mathbf{w}} \in \hat{X}_N. \quad (3.16)$$

We thus find the $\hat{\mathbf{v}}_i$'s by solving (3.16) for the precomputed $\hat{p}_i, i = 1, \dots, N$. In practice, we evaluate the integrals in (3.16) using GLL quadrature. We define the enriched velocity reference space as

$$\hat{X}_N^e = \text{span}\{\hat{\mathbf{v}}_i, \quad i = 1, \dots, N\}, \quad (3.17)$$

with corresponding enriched velocity space defined on Ω as

$$X_N^e = \text{span}\{ \mathcal{I}_N(\Psi^{-1}(\hat{\mathbf{v}}_i) \circ \Phi) \circ \Phi^{-1}, \quad i = 1, \dots, N \}. \quad (3.18)$$

If we then define

$$X_N = X_N^0 \oplus X_N^e, \quad (3.19)$$

the inf-sup condition will be satisfied since

$$\inf_{\hat{q} \in \hat{M}_N} \sup_{\hat{\mathbf{u}} \in \hat{X}_N^0 \oplus \hat{X}_N^e} \frac{\int_{\hat{\Omega}} \hat{q} \hat{\nabla} \cdot \hat{\mathbf{u}} d\hat{\Omega}}{\|\hat{q}\|_{L^2} \|\hat{\mathbf{u}}\|_{H^1}} \geq \inf_{\hat{q} \in \hat{M}_N} \sup_{\hat{\mathbf{u}} \in \hat{X}_N^e} \frac{\int_{\hat{\Omega}} \hat{q} \hat{\nabla} \cdot \hat{\mathbf{u}} d\hat{\Omega}}{\|\hat{q}\|_{L^2} \|\hat{\mathbf{u}}\|_{H^1}} = \inf_{\hat{q} \in \hat{M}_N} C \frac{|\hat{\mathbf{v}}(\hat{q})|_{H^1}}{\|\hat{q}\|_{L^2}} = \beta > 0, \quad (3.20)$$

where C is a constant, and $\hat{\mathbf{v}}(\hat{q})$ is the solution of (3.16) with $\hat{p} = \hat{q}$. We remark that β may depend on N .

3.4. Method 2

In our second method we will explicitly use the fact that the basis functions in X_N^0 are almost divergence free. It is well known that the solution of the steady Stokes problem (2.17) corresponds to solving an underlying min-max problem; see [7]. With the availability of a divergence free basis, this min-max problem reduces to the pure minimization problem

$$\mathbf{u}_N = \arg \min_{\mathbf{v} \in V_N} I(\mathbf{v}) = \frac{1}{2} a_N(\mathbf{v}, \mathbf{v}) - l_N(\mathbf{v}),$$

where

$$V_N = \{\mathbf{v} \in X_N, \quad b_N(\mathbf{v}, q) = 0 \quad \forall q \in \mathcal{M}_N\}.$$

This minimization problem is again equivalent to the (vector) Poisson problem: Find $\mathbf{u}_N \in V_N$ such that

$$a_N(\mathbf{u}_N, \mathbf{v}) = l_N(\mathbf{v}) \quad \forall \mathbf{v} \in V_N. \quad (3.21)$$

To solve this Poisson-type problem the inf-sup condition is irrelevant, and (3.21) has a unique solution $\mathbf{u}_N \in V_N$ due to the coercivity of $a_N(\cdot, \cdot)$.

Method 2 then consists of approximating V_N by X_N^0 and instead solve the problem: Find $\mathbf{u}_N \in X_N^0$ such that

$$a_N(\mathbf{u}_N, \mathbf{v}) = l_N(\mathbf{v}) \quad \forall \mathbf{v} \in X_N^0. \quad (3.22)$$

The advantage of this approach lies in the fact that the resulting algebraic system is very small. In fact, the dimension of this system is just N . An extension of this approach to three dimensions would also yield a system of dimension N for N precomputed basis functions.

The solution of (3.22) only gives the velocity. In order to compute the pressure, we proceed as follows: We know that for all $\mathbf{v} \in V_{\mathcal{N}}$, $b_{\mathcal{N}}(\mathbf{v}, q) = 0 \quad \forall q \in M_{\mathcal{N}}$. On the other hand, for Method 2 we know that for all $\mathbf{v} \in X_{\mathcal{N}}^0$, $b_{\mathcal{N}}(\mathbf{v}, q)$ will be approximately equal to zero for all $q \in M_{\mathcal{N}}$; see (3.14). Besides, we know that the inf-sup condition is fulfilled for the previously defined spaces $X_{\mathcal{N}}^e$ and $M_{\mathcal{N}}$. We can then compute the pressure $p_{\mathcal{N}} \in M_{\mathcal{N}}$ uniquely by solving

$$b_{\mathcal{N}}(\mathbf{v}, p_{\mathcal{N}}) = -a_{\mathcal{N}}(\mathbf{u}_{\mathcal{N}}, \mathbf{v}) + l_{\mathcal{N}}(\mathbf{v}) \quad \forall \mathbf{v} \in X_{\mathcal{N}}^e. \quad (3.23)$$

The dimension of the algebraic system corresponding to (3.23) is just N , similar to the velocity system.

3.5. Relation between Method 1 and Method 2

Since the ability to work with divergence free functions is tempting, let us make a few remarks that will allow us to better understand the links between the two methods.

First, one could imagine to modify the basis functions $\tilde{\mathbf{u}}_i$ so that these are exactly divergence free, at least in the reduced basis sense. To do that, let us first compute corrections $\mathbf{u}'_i \in X_{\mathcal{N}}^e$ so that

$$b_{\mathcal{N}}(\mathbf{u}'_i, q) = b_{\mathcal{N}}(\tilde{\mathbf{u}}_i, q) \quad \forall q \in M_{\mathcal{N}}.$$

The existence of \mathbf{u}'_i follows from the inf-sup condition and $\dim(M_{\mathcal{N}}) = \dim(X_{\mathcal{N}}^e)$, with the norm of \mathbf{u}'_i presumably bounded by $C \|\mathbf{u}_i - \mathbf{u}^i\|_{H^1(\Omega_i)}$, and with C depending on β . Based on $\check{\mathbf{u}}_i = \tilde{\mathbf{u}}_i - \mathbf{u}'_i$ we could then define a space

$$\check{X}_{\mathcal{N}}^0 = \text{span}\{\check{\mathbf{u}}_i, \quad i = 1, \dots, N\}$$

so that

$$\forall \mathbf{v} \in \check{X}_{\mathcal{N}}^0, \quad b_{\mathcal{N}}(\mathbf{v}, q) = 0 \quad \forall q \in M_{\mathcal{N}}.$$

We could then propose a method based on $\check{X}_{\mathcal{N}}^0$ following (3.22) named Method $\check{2}$.

Second, it is interesting to note that Method 1 and Method $\check{2}$ now coincide, which can be seen as follows. Although $\mathbf{u}_{\mathcal{N}}$ according to Method 1 is an element in $X_{\mathcal{N}}^0 \oplus X_{\mathcal{N}}^e$, we will argue that $\mathbf{u}_{\mathcal{N}} \in \check{X}_{\mathcal{N}}^0$. First we let

$$\mathbf{u}_{\mathcal{N}} = \check{\mathbf{u}}_{\mathcal{N}}^0 + \sum_{i=1}^N \alpha_i \mathbf{v}_i, \quad (3.24)$$

where $\check{\mathbf{u}}_{\mathcal{N}}^0 \in \check{X}_{\mathcal{N}}^0$, and $\mathbf{v}_i \in X_{\mathcal{N}}^e$ for $i = 1, \dots, N$. This gives the relation

$$b_{\mathcal{N}}(\mathbf{u}_{\mathcal{N}}, q) = b_{\mathcal{N}}\left(\sum_{i=1}^N \alpha_i \mathbf{v}_i, q\right) \quad \forall q \in M_{\mathcal{N}}. \quad (3.25)$$

Next we take $q = \sum_{i=1}^N \alpha_i p_i$, where $\{p_i\}_{i=1}^N$ is the basis for $M_{\mathcal{N}}$, and get

$$b_{\mathcal{N}}(\mathbf{u}_{\mathcal{N}}, q) = b_{\mathcal{N}}\left(\sum_{i=1}^N \alpha_i \mathbf{v}_i, \sum_{i=1}^N \alpha_i p_i\right), \quad (3.26)$$

which according to (3.16) leads to

$$b_{\mathcal{N}}(\mathbf{u}_{\mathcal{N}}, q) = a_{\mathcal{N}}\left(\sum_{i=1}^N \alpha_i \mathbf{v}_i, \sum_{i=1}^N \alpha_i \mathbf{v}_i\right) \geq 0. \quad (3.27)$$

We already know that

$$b_{\mathcal{N}}(\mathbf{u}_{\mathcal{N}}, q) = 0 \quad \forall q \in M_{\mathcal{N}}, \quad (3.28)$$

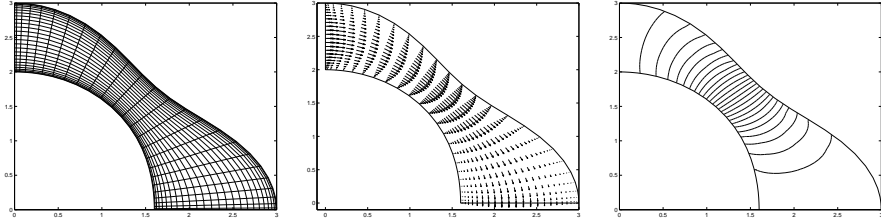


FIGURE 2. The domain Ω with velocity and pressure solution.

so we must have $\sum_{i=1}^N \alpha_i \mathbf{v}_i = 0$, which again means that $\alpha_i = 0$ for $i = 1, \dots, N$ since the \mathbf{v}_i 's are linearly independent, which follows directly from the linear independence of the p_i 's. Hence, $\mathbf{u}_N \in \tilde{X}_N^0 \subset X_N$. Method 1 and Method $\hat{2}$ are thus equivalent (at least for the single domain case considered here), however, the two methods lead to different computational schemes with different computational complexities.

Third, we expect Method 2 and Method $\hat{2}$ to give very similar velocity fields. This remark is justified heuristically by the fact that $\tilde{\mathbf{u}}_i$ and $\check{\mathbf{u}}_i$ differ with a very small amount (they are "spectrally close", i.e., the error is based on the spectral accuracy $\|\mathbf{u}_i - \mathbf{u}^i\|_{H^1}$ and not on the reduced basis accuracy). This claim is also substantiated by numerical evidence since Method 1 and Method 2 give almost the same convergence rate; see for example the numerical results reported in Table 1 in the context of a simple geometric framework. However, the results from Method 2 may not always be as good as the results from Method 1, in particular, when the reduced basis error is very small.

Finally, we remark that for both methods, the exact (spectral) solution is recovered on the geometries that have been used to build the reduced basis (consistency of the approach), and also on the geometries obtained through symmetry acting on these geometries.

3.6. Numerical results

We now define the domain $\Omega = \Phi(\hat{\Omega})$ to be the deformed annulus in Figure 2. For a polynomial degree $\mathcal{N} = 25$ we compute the solution $(\mathbf{u}_{\mathcal{N}}, p_{\mathcal{N}})$ of (2.17), and use it to assess the quality of our reduced basis approximation (\mathbf{u}_N, p_N) . The velocity and pressure functions $\{(\mathbf{u}_i, p_i) \in X_{\mathcal{N}}(\Omega_i) \times M_{\mathcal{N}}(\Omega_i)\}_{i=1}^8$ are found by solving (2.17) on the different geometries appearing in Figure 3. After mapping these functions to the reference domain as $\hat{p}_i = p_i \circ \Phi_i$ and $\hat{\mathbf{u}}_i = \Psi_i(\mathbf{u}_i)$, $i = 1, \dots, 8$, we have obtained the first eight basis functions. The velocity and pressure basis functions 2 through 8 are then reflected across the horizontal center line on the reference domain to produce basis functions 9 through 15, i.e. $N = 15$. Finally, for each pressure basis function, one additional velocity basis function is constructed according to (3.16) to enrich the velocity basis. A precise definition of Ω and $\{\Omega_i\}_{i=1}^8$ is given in [14], where a scalar Poisson problem is solved with the reduced basis method using the same deformed geometries.

We use Method 1 for compatible spaces X_N and M_N to solve the steady Stokes equations (3.9) in the reduced basis context for different values of N . These results are presented in Table 1. We clearly see in Table 1 that the error between $\mathbf{u}_N \in X_N$ and $\mathbf{u}_{\mathcal{N}} \in X_{\mathcal{N}}$ decreases as N grows. Similar to the results for the scalar Poisson problem studied in [14], the reduced basis method gives good results also for incompressible vector fields.

The pressure solution is a scalar field, and we see that it converges somewhat faster than the velocity. We would like exponential convergence both for velocity and pressure, but if we study the results in Table 1 for $N = 1, \dots, 4$, the convergence is very slow. For $N = 5, \dots, 8$, however, the convergence is very good. A natural explanation for this is that the first four basis functions in X_N and M_N are constructed from the solutions of (3.9) on squares with deformed lower edges, see Figure 3. Since Ω is a deformed annulus, the next four basis functions approximate the solution better. The effect of using only the four basis functions constructed from the deformed annuli in Figure 3 is shown in Figures 4(a) and 4(b). From this it is easy to see that a good choice of domains Ω_i is essential in order to make our method effective. How to make this choice for a generic Ω will

N	$\ \mathbf{u}_N - \mathbf{u}_N\ _{H^1}$	$\ p_N - p_N\ _{L^2}$
1	$1.7 \cdot 10^{-2}$	$2.3 \cdot 10^{-1}$
2	$1.4 \cdot 10^{-2}$	$1.7 \cdot 10^{-1}$
3	$1.2 \cdot 10^{-2}$	$1.6 \cdot 10^{-1}$
4	$1.2 \cdot 10^{-2}$	$1.6 \cdot 10^{-1}$
5	$8.8 \cdot 10^{-3}$	$1.0 \cdot 10^{-1}$
6	$8.6 \cdot 10^{-3}$	$5.2 \cdot 10^{-2}$
7	$3.2 \cdot 10^{-3}$	$1.9 \cdot 10^{-2}$
8	$2.7 \cdot 10^{-3}$	$1.8 \cdot 10^{-2}$
9	$2.6 \cdot 10^{-3}$	$1.4 \cdot 10^{-2}$
10	$2.0 \cdot 10^{-3}$	$9.7 \cdot 10^{-3}$
11	$2.0 \cdot 10^{-3}$	$9.7 \cdot 10^{-3}$
12	$1.8 \cdot 10^{-3}$	$9.5 \cdot 10^{-3}$
13	$1.7 \cdot 10^{-3}$	$9.3 \cdot 10^{-3}$
14	$1.4 \cdot 10^{-3}$	$9.2 \cdot 10^{-3}$
15	$1.4 \cdot 10^{-3}$	$8.6 \cdot 10^{-3}$

TABLE 1. Convergence results for Method 1. The dimension of X_N is $2N$, while the dimension of X_N^0 is N .

be addressed in a later paper. The approach consists in combining the *a posteriori* tool presented in the next section in a recursive manner. This “greedy approach” follows the paper [19].

The results for Method 2 are almost identical to the results presented for Method 1 in Table 1. The main difference between the two approaches lies in the computational complexity associated with solving the resulting algebraic systems. In Method 1 we solve a coupled Stokes system involving $2N$ degrees of freedom for the velocity and N degrees of freedom for the pressure. In Method 2 we first solve a system of dimension N for the velocity and then a system of dimension N for the pressure. In fact, if we don’t need the pressure solution, Method 2 permits us to only solve the velocity system of dimension N .

Linear independence of the basis functions can generally be expected in most practical cases. However, some of the basis functions may be nearly linearly dependent, and this issue can be controlled by using an orthogonalization procedure. The orthogonalization also greatly reduces conditioning issues associated with the resulting systems of algebraic equations. For the velocity, orthogonalization is done on $\hat{\Omega}$ with respect to

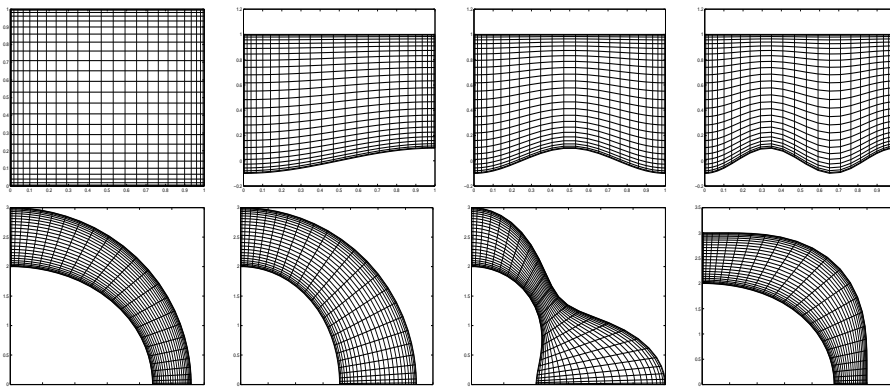
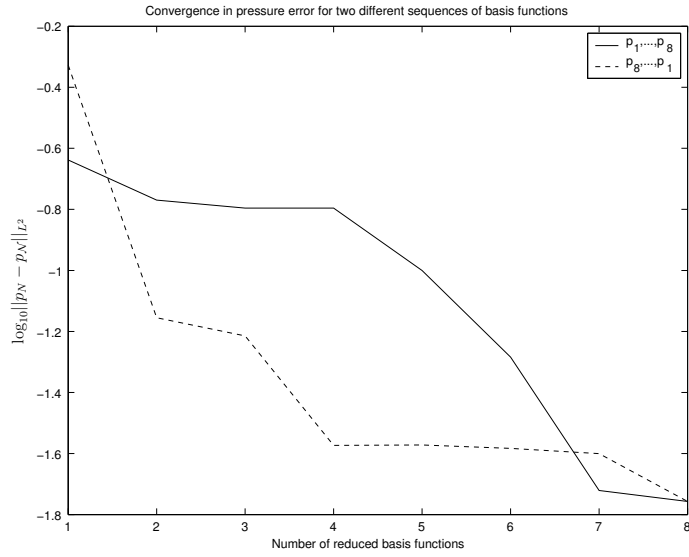
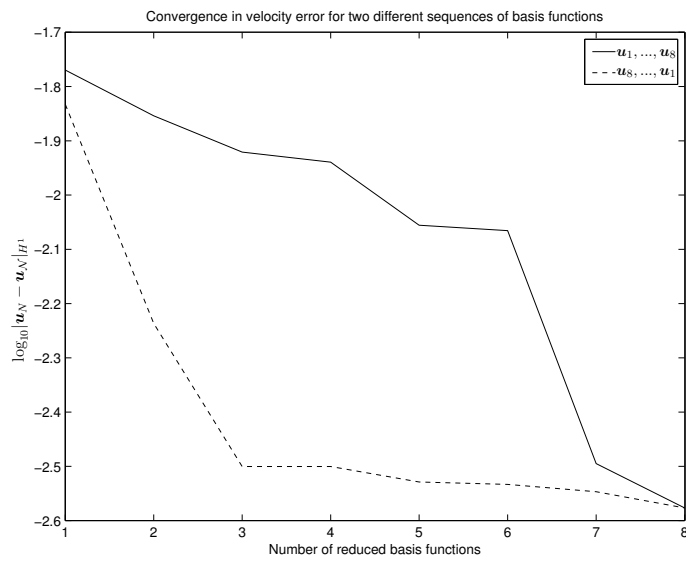


FIGURE 3. The deformed geometries used to construct the basis functions.



(a) Pressure



(b) Velocity

FIGURE 4. The effect of changing the order of the basis functions (Method 1).

$a_{\mathcal{N}}(\cdot, \cdot)$, while the pressure is orthogonalized with respect to the discrete L^2 inner product. Since this is done on the reference domain it is part of the preprocessing stage. Note that in order to preserve the divergence free property of the original velocity basis functions, the orthogonalization must be done after ordering the basis functions in a proper way. First we orthogonalize the elements in X_N^0 , followed by the elements in X_N^e .

For the fully coupled system of Method 1, the corresponding Uzawa pressure operator can be constructed explicitly, and the smallest eigenvalue of this operator is directly connected to the inf-sup parameter β ; see [10]. By computing numerically the minimum eigenvalue and the condition number of the Uzawa pressure operator, the numerical results indicate that these are constant for our problem and equal to $7.3 \cdot 10^{-2}$ and 14, respectively, independent of N (at least for the range of values we are dealing with).

3.7. *A posteriori* error estimation

In order to assess the quality of our reduced basis method we need *a posteriori* error estimation. For some specified output of interest, $s(\mathbf{u})$, it will consist in providing lower and upper output bounds $s^-(\mathbf{u}_N)$ and $s^+(\mathbf{u}_N)$, such that

$$s^-(\mathbf{u}_N) \lesssim s(\mathbf{u}) \lesssim s^+(\mathbf{u}_N), \quad (3.29)$$

where $a \lesssim b$ means that $a - b \ll \varepsilon_{\mathcal{N}}$. In this work, we focus on a compliant output, i.e.

$$s(\mathbf{u}) = l(\mathbf{u}). \quad (3.30)$$

The hypothesis made on the spectral method is that $|s(\mathbf{u}) - s(\mathbf{u}_N)| \ll \varepsilon_{\mathcal{N}}$.

The following derivation is based on the solution provided by Method 1. We will follow the theory developed in [16] for operators which are continuous, coercive, symmetric and affine in terms of the parameter, in the similar way as has been done in [18] for the steady Stokes problem for more standard parameter dependencies. The steady Stokes operator is symmetric and continuous, but not coercive, and due to the geometric parameter it is not affine either.

We introduce the diffusion operator

$$\hat{a}(\mathbf{v}, \mathbf{w}) = \int_{\hat{\Omega}} g(\Phi) \hat{\nabla}(\mathbf{v} \circ \Phi) \cdot \hat{\nabla}(\mathbf{w} \circ \Phi) d\hat{\Omega}, \quad (3.31)$$

on the reference domain, where $g(\Phi)$ is a geometry dependent positive function. The reconstructed error $\mathbf{e} \in \tilde{X}_{\mathcal{N}}$ is then defined as the field that for some $g(\Phi)$ satisfies

$$\hat{a}(\mathbf{e}, \mathbf{v}) = l(\mathbf{v}) - a(\mathbf{u}_N, \mathbf{v}) - b(\mathbf{v}, p_N) \quad \forall \mathbf{v} \in \tilde{X}_{\mathcal{N}}, \quad (3.32)$$

where $\tilde{X}_{\mathcal{N}} = \{\mathbf{v} \circ \Phi \in (\mathbb{P}_{\mathcal{N}}(\hat{\Omega}))^2, \mathbf{v}|_{\Gamma_w} = 0\}$. The operator $g(\Phi)$ is chosen such that

$$\alpha_0 \|\mathbf{v}\|_{X_{\mathcal{N}}}^2 \leq \hat{a}(\mathbf{v}, \mathbf{v}) \leq a(\mathbf{v}, \mathbf{v}) \quad \forall \mathbf{v} \in X_{\mathcal{N}}, \quad (3.33)$$

for some positive real constant α_0 . For this reconstructed error we claim that

$$s^-(\mathbf{u}_N) = l(\mathbf{u}_N), \text{ and} \quad (3.34)$$

$$s^+(\mathbf{u}_N) = l(\mathbf{u}_N) + \hat{a}(\mathbf{e}, \mathbf{e}) \quad (3.35)$$

are lower and upper bounds for the exact output $s(\mathbf{u})$ up to spectral accuracy. We remark that we throughout this section will drop the subscript \mathcal{N} indicating that we actually evaluate all the bilinear and linear forms using GLL quadrature.

Before we prove (3.34) and (3.35), we put $\mathbf{v} = \mathbf{u}_N$ in (2.17) and (3.9) to derive that

$$a(\mathbf{u}_N, \mathbf{u}_N - \mathbf{u}_N) + b(\mathbf{u}_N, p_N) = 0. \quad (3.36)$$

For the lower bound we now get

$$\begin{aligned}
s^-(\mathbf{u}_N) &= s(\mathbf{u}_N) + l(\mathbf{u}_N - \mathbf{u}_N) \\
&= s(\mathbf{u}_N) + a(\mathbf{u}_N, \mathbf{u}_N - \mathbf{u}_N) + b(\mathbf{u}_N - \mathbf{u}_N, p_N) \\
&= s(\mathbf{u}_N) + a(\mathbf{u}_N, \mathbf{u}_N - \mathbf{u}_N) + b(\mathbf{u}_N, p_N) \\
&= s(\mathbf{u}_N) + a(\mathbf{u}_N, \mathbf{u}_N - \mathbf{u}_N) + a(\mathbf{u}_N, \mathbf{u}_N - \mathbf{u}_N) + 2b(\mathbf{u}_N, p_N) \\
&= s(\mathbf{u}_N) + a(\mathbf{u}_N - \mathbf{u}_N, \mathbf{u}_N - \mathbf{u}_N) + 2b(\mathbf{u}_N, p_N).
\end{aligned} \tag{3.37}$$

It follows that

$$s^-(\mathbf{u}_N) \leq s(\mathbf{u}_N) + 2b(\mathbf{u}_N, p_N) \tag{3.38}$$

independent of $g(\Phi)$, and hence,

$$s^-(\mathbf{u}_N) \lesssim s(\mathbf{u}) + 2b(\mathbf{u}_N, p_N). \tag{3.39}$$

For the upper bound we denote the error on the deformed domain by $\mathbf{e}^u = \mathbf{u}_N - \mathbf{u}_N$, and find that

$$\begin{aligned}
2\hat{a}(\mathbf{e}, \mathbf{e}^u) &= l(\mathbf{u}_N - \mathbf{u}_N) + l(\mathbf{u}_N - \mathbf{u}_N) \\
&\quad - 2a(\mathbf{u}_N, \mathbf{u}_N - \mathbf{u}_N) - 2b(\mathbf{u}_N, p_N) \\
&= l(\mathbf{u}_N - \mathbf{u}_N) + a(\mathbf{u}_N, \mathbf{u}_N - \mathbf{u}_N) \\
&\quad + b(\mathbf{u}_N - \mathbf{u}_N, p_N) - 2a(\mathbf{u}_N, \mathbf{u}_N - \mathbf{u}_N) - 2b(\mathbf{u}_N, p_N) \\
&= l(\mathbf{u}_N - \mathbf{u}_N) + a(\mathbf{u}_N - \mathbf{u}_N, \mathbf{u}_N - \mathbf{u}_N) \\
&\quad - a(\mathbf{u}_N, \mathbf{u}_N - \mathbf{u}_N) - b(\mathbf{u}_N, p_N) - 2b(\mathbf{u}_N, p_N) \\
&= l(\mathbf{u}_N - \mathbf{u}_N) + a(\mathbf{e}^u, \mathbf{e}^u) - 2b(\mathbf{u}_N, p_N).
\end{aligned} \tag{3.40}$$

To prove that (3.35) is an upper bound we now use (3.40) to get

$$\begin{aligned}
s^+(\mathbf{u}_N) &= l(\mathbf{u}_N) + \hat{a}(\mathbf{e}, \mathbf{e}) \\
&= l(\mathbf{u}_N) + \hat{a}(\mathbf{e}, \mathbf{e}) \\
&\quad - 2\hat{a}(\mathbf{e}, \mathbf{e}^u) + l(\mathbf{u}_N - \mathbf{u}_N) + a(\mathbf{e}^u, \mathbf{e}^u) - 2b(\mathbf{u}_N, p_N) \\
&\quad + \hat{a}(\mathbf{e}^u, \mathbf{e}^u) - \hat{a}(\mathbf{e}^u, \mathbf{e}^u) \\
&= l(\mathbf{u}_N) + \hat{a}(\mathbf{e} - \mathbf{e}^u, \mathbf{e} - \mathbf{e}^u) - 2b(\mathbf{u}_N, p_N) \\
&\quad + a(\mathbf{e}^u, \mathbf{e}^u) - \hat{a}(\mathbf{e}^u, \mathbf{e}^u) \\
&\geq s(\mathbf{u}_N) - 2b(\mathbf{u}_N, p_N),
\end{aligned} \tag{3.41}$$

where the inequality is due to (3.33) and the coercivity of $\hat{a}(\cdot, \cdot)$. Hence, for the upper bound we have

$$s^+(\mathbf{u}_N) \gtrsim s(\mathbf{u}) - 2b(\mathbf{u}_N, p_N). \tag{3.42}$$

To conclude, we notice that $b(\mathbf{u}_N, p_N) = b(\mathbf{u}_N, p_N - p_N)$, and by using (3.14) and Cachy-Schwarz, this term is upper bounded by $\varepsilon_N \|p - p_N\|_{L^2} \ll \varepsilon_N$.

It now remains to find a positive function $g(\Phi)$, such that

$$a(\mathbf{v}, \mathbf{v}) \geq \hat{a}(\mathbf{v}, \mathbf{v}) \quad \forall \mathbf{v} \in X_N. \tag{3.43}$$

For a constant $g(\Phi) = \lambda$, we can use the theory of [16] to see that λ should be chosen as large as possible without violating (3.43). This largest constant may be found, as in [14], by computing the smallest eigenvalue of the generalized symmetric eigenvalue problem

$$a(\mathbf{v}, \mathbf{v}) = \lambda \int_{\hat{\Omega}} \hat{\nabla}(\mathbf{v} \circ \Phi) \cdot \hat{\nabla}(\mathbf{v} \circ \Phi) d\hat{\Omega}. \tag{3.44}$$

We tried this approach also for the current problem, and used an inverse Rayleigh quotient iteration to estimate λ , but the resulting upper bound gap proved much too conservative.

To get a better estimate we consider the Jacobian, $\mathcal{J}(\Phi)$, of the mapping from $\hat{\Omega}$ to Ω . We start with the left hand side of (3.43), and use the fact that

$$\nabla = \mathcal{J}^{-T} \hat{\nabla} \quad (3.45)$$

to rewrite (2.4), like we did in (2.10), to get

$$\begin{aligned} a(\mathbf{v}, \mathbf{v}) &= \int_{\hat{\Omega}} (\hat{\nabla}(\mathbf{v} \circ \Phi))^T \mathcal{J}^{-1} \mathcal{J}^{-T} \hat{\nabla}(\mathbf{v} \circ \Phi) |J| d\hat{\Omega} \\ &= \int_{\hat{\Omega}} \mathbf{w}^T G \mathbf{w} d\hat{\Omega}, \end{aligned} \quad (3.46)$$

where $\mathbf{w} = \hat{\nabla}[\mathbf{v} \circ \Phi]$ and $G = G(\Phi) = (\mathcal{J}^T \mathcal{J})^{-1} |J|$. At each point $\hat{\mathbf{x}} \in \hat{\Omega}$ we diagonalize the 2×2 symmetric positive-definite matrix G , that is, we write $G(\Phi(\hat{\mathbf{x}})) = Q^T \Lambda Q$, where Q consists of the orthonormal eigenvectors of G . If we (at each point $\hat{\mathbf{x}} \in \hat{\Omega}$) replace the two diagonal elements of Λ with the smallest one, Λ_{min} , we get

$$\int_{\hat{\Omega}} \mathbf{w}^T G \mathbf{w} d\hat{\Omega} \geq \int_{\hat{\Omega}} \Lambda_{min} (Q\mathbf{w})^T Q\mathbf{w} d\hat{\Omega}. \quad (3.47)$$

Since Q consists of the orthonormal eigenvectors, the last expression is equivalent to $\int_{\hat{\Omega}} \Lambda_{min} \mathbf{w}^T \mathbf{w} d\hat{\Omega}$, and we end up with

$$a(\mathbf{v}, \mathbf{v}) \geq \int_{\hat{\Omega}} \Lambda_{min} \hat{\nabla}(\mathbf{v} \circ \Phi) \cdot \hat{\nabla}(\mathbf{v} \circ \Phi) d\hat{\Omega}. \quad (3.48)$$

This is just (3.31) with $g(\Phi) = \Lambda_{min}(\Phi)$, and thus (3.43) is satisfied.

If we replace $\Lambda_{min}(\Phi)$ by $\bar{\Lambda}_{min}(\Phi) = \min_{\hat{\mathbf{x}} \in \hat{\Omega}} \Lambda_{min}(\Phi)$, we may put $g(\Phi)$ outside the integral and apply the theory of [16]. This will produce a more conservative upper bound, but the calculation of (3.35) can then be split in an off-line/on-line procedure.

We remark that it is important to obtain computable upper and lower bounds with spectral accuracy, and it is imperative that the bound gap $s_N^+ - s_N^-$ goes to zero very fast as $N \rightarrow \infty$. It is a result of (3.37) and (3.41) that the latter is indeed the case since $s_N^+ - s_N^-$ behaves like $\|u - u_N\|_{H^1}^2$.

3.8. Numerical results for the output bounds

To compute the output bounds numerically, we will use the domain $\Omega = \Phi(\hat{\Omega})$ defined in Figure 2. The basis functions for X_N and M_N are computed according to Section 3.6, which gives us 15 basis functions for X_N^0 , X_N^e and M_N .

The upper bound for $g(\Phi) = \Lambda_{min}(\Phi)$ is denoted s^+ , while the upper bound for the constant $g(\Phi) = \bar{\Lambda}_{min}(\Phi)$ is denoted s_2^+ . The results for the previously defined deformed geometry are presented in Table 2. In Figure 5 we present the same results graphically, and in addition we compare the results with $a(\mathbf{u}_N - \mathbf{u}_N, \mathbf{u}_N - \mathbf{u}_N)$. As we should expect from (3.37), Figure 5 confirms that $s(\mathbf{u}_N) - s^-(\mathbf{u}_N) \approx a(\mathbf{u}_N - \mathbf{u}_N, \mathbf{u}_N - \mathbf{u}_N)$. The slight deviation that can be seen for some N is on the order of 10^{-10} , which is smaller than the stopping criterion in the iterative method used to find the basis functions; see Section 2.3. From Figure 5 we also see that s_2^+ is very close to s^+ . Thus the approximation of $\Lambda_{min}(\Phi)$ by a constant does not deteriorate the upper bound considerably in the case we have tested so far.

From both Table 2 and Figure 5 we see that the upper bound gap is relatively large compared to the lower bound gap. In the future, a different method to find an improved estimate of $g(\Phi)$ is desirable to reduce the upper bound gap.

4. A REDUCED BASIS ELEMENT METHOD

We will in this section extend the tools developed for a single domain to multiple domains. This is done to provide enough geometrical flexibility in the solvers, and we get either a spectral element method or a reduced

N	$s(\mathbf{u}_N) - s^-(\mathbf{u}_N)$	$s^+(\mathbf{u}_N) - s(\mathbf{u}_N)$	$s_2^+(\mathbf{u}_N) - s(\mathbf{u}_N)$
1	$2.82 \cdot 10^{-4}$	$5.28 \cdot 10^{-2}$	$1.01 \cdot 10^{-1}$
2	$1.87 \cdot 10^{-4}$	$9.86 \cdot 10^{-2}$	$1.85 \cdot 10^{-1}$
3	$1.35 \cdot 10^{-4}$	$9.74 \cdot 10^{-2}$	$1.90 \cdot 10^{-1}$
4	$1.32 \cdot 10^{-4}$	$9.70 \cdot 10^{-2}$	$1.86 \cdot 10^{-1}$
5	$7.67 \cdot 10^{-5}$	$3.02 \cdot 10^{-2}$	$4.52 \cdot 10^{-2}$
6	$7.44 \cdot 10^{-5}$	$6.86 \cdot 10^{-3}$	$1.20 \cdot 10^{-2}$
7	$1.04 \cdot 10^{-5}$	$1.56 \cdot 10^{-3}$	$2.60 \cdot 10^{-3}$
8	$7.03 \cdot 10^{-6}$	$2.62 \cdot 10^{-3}$	$4.32 \cdot 10^{-3}$
9	$7.02 \cdot 10^{-6}$	$1.61 \cdot 10^{-3}$	$2.39 \cdot 10^{-3}$
10	$4.24 \cdot 10^{-6}$	$6.10 \cdot 10^{-4}$	$1.02 \cdot 10^{-3}$
11	$4.16 \cdot 10^{-6}$	$6.21 \cdot 10^{-4}$	$1.05 \cdot 10^{-3}$
12	$3.15 \cdot 10^{-6}$	$6.16 \cdot 10^{-4}$	$9.68 \cdot 10^{-4}$
13	$2.82 \cdot 10^{-6}$	$4.63 \cdot 10^{-4}$	$7.50 \cdot 10^{-4}$
14	$1.94 \cdot 10^{-6}$	$4.32 \cdot 10^{-4}$	$6.97 \cdot 10^{-4}$
15	$1.94 \cdot 10^{-6}$	$3.82 \cdot 10^{-4}$	$6.71 \cdot 10^{-4}$

TABLE 2. Convergence of the lower and the upper bound gaps. Here, s^+ corresponds to the variable $g(\Phi) = \Lambda_{min}(\Phi)$, while s_2^+ corresponds to the constant $g(\Phi) = \bar{\Lambda}_{min}(\Phi)$.

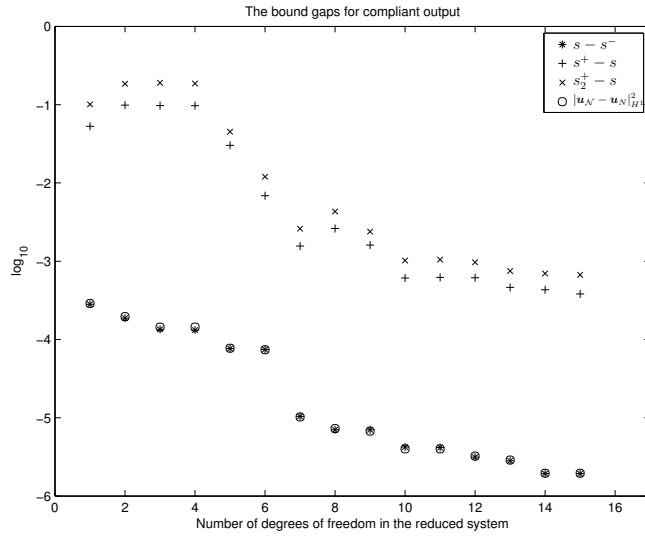


FIGURE 5. The bound gaps.

basis element method. By dividing the domain into separate subdomains, we may also exploit parallel processing techniques. For K subdomains the decomposition is performed in a non-overlapping way such that $\Omega = \cup_{k=1}^K \Omega_k$. For simplicity, the domain is only decomposed in the flow direction. In this way the inlet boundary will be entirely in one subdomain, the outflow boundary in another, and all other subdomains will have only two neighbouring subdomains. On the interface $\bar{\Gamma}_{kl} = \bar{\Omega}_k \cap \bar{\Omega}_l$ between two neighbouring subdomains, the pressure may be discontinuous since it is only required to be in L^2 . We use a conforming spectral element method to

generate the reference solution (\mathbf{u}_N, p_N) on multiple domains. The velocity \mathbf{u}_N is then in H^1 and the reduced basis element solution \mathbf{u}_N should thus be continuous in all of Ω . This continuity is generally not possible to achieve exactly across the interfaces, and we get a nonconforming method with consistency error

$$\sum_{k,l} \int_{\Gamma_{kl}} \left(\nu \frac{\partial \mathbf{u}_N}{\partial \mathbf{n}} - p_N \mathbf{n} \right) \cdot (\mathbf{u}_N|_{\Omega_k} - \mathbf{u}_N|_{\Omega_l}) ds. \quad (4.1)$$

In the spirit of the mortar element method, we will minimize the jump across the interfaces through Lagrange multipliers; see [3] and [4].

4.1. Precomputing the basis functions

In the single domain case we constructed precomputed velocity basis functions with zero tangential velocity on the inlet and outflow boundaries, and precomputed pressure basis functions which all were close to one on the inlet boundary and zero on the outflow boundary. In the case of multiple subdomains, we need reduced basis functions with good approximation properties along the internal interfaces. To achieve this, we use two alternative approaches.

In the first approach we solve the steady Stokes problem on the eight predefined geometries using two subdomains. The restriction of these solutions to the subdomain associated with the outflow boundary comprise our initial basis functions. On the reference domain these functions are flipped across the horizontal axis ($\eta = 0$) to produce their symmetric variants. The solution on the undeformed square is not flipped, since it is symmetric already, and we thus get $N = 15$ basis functions for both the pressure and the velocity. To represent the solution on the inlet subdomain and on central subdomains, the functions are reflected across the vertical axis ($\xi = 0$) on the reference domain. Thus we get a total of $2N = 30$ available basis functions from the first approach. All the $2N$ basis functions will be used on interior subdomains, while only half of these will be used on the subdomains corresponding to the inlet and outflow subdomains. In addition, one pressure basis function with a constant value equal to one will be used on the inlet subdomain in order to raise the level of the pressure solution on this subdomain. Since we use the restriction of the precomputed solutions to the outflow subdomain, all the pressure basis functions have values close to zero on the outflow edge. Without the additional constant function, this approximation is insufficient on the inlet domain. Alternatively, the reflected basis functions may be added for the inlet subdomain, but then more than one additional basis function is needed.

In the second approach we solve the steady Stokes problem on the eight predefined geometries using three subdomains instead of two. Now we use the restriction of the solutions to each of the subdomains as basis functions in similar subdomains in the generic problem. The idea is that the solution restricted to the inlet subdomain better represents what happens on the inlet subdomain in the generic problem, and similarly for the other subdomains. After flipping on the reference domain this approach produces a total of $3N = 45$ basis functions for both the pressure and the velocity. In the second approach there is no need to reflect the basis functions across the vertical axis. There is also no need to use an additional constant pressure function on the inlet subdomain, since the restrictions of the pressure solutions to the inlet subdomain are clearly non-zero on all edges. Following this approach we will thus use N basis functions to approximate the pressure on the inlet subdomain, and N basis functions on any interior subdomain, and N basis functions on the outflow subdomain. A similar procedure is used to approximate the velocity.

To ensure stability of the reduced basis element solution, all basis functions are orthogonalized, but we keep the basis functions representing different subdomains separated. For the pressure basis functions the orthogonalization is done with respect to the discrete L^2 inner product on the reference domain. The velocity basis functions are orthogonalized with respect to $a_N(\cdot, \cdot)$ on the reference domain, while imposing the boundary conditions corresponding to the subdomain the given velocity basis function represents.

In both Method 1 and Method 2 we have to enrich the velocity basis in order to find both the pressure and the velocity solution in the reduced basis element context. In Method 1 it is crucial that the inf-sup condition is fulfilled, and we use the same technique as for the single-domain case to produce one additional velocity basis

function for each pressure basis function. Again, the correct boundary conditions have to be used, according to which subdomain the velocity basis function represents. In Method 2 these additional velocity basis functions are used in the computation of the pressure solution only.

Using the first approach to construct the precomputed basis functions we define

$$\begin{aligned}\hat{X}_N = X_N(\hat{\Omega}) &= \begin{cases} \text{span}\{\hat{\mathbf{u}}_i, & i = 2N+1, \dots, 4N+1\}, & k = 1 \\ \text{span}\{\hat{\mathbf{u}}_i, & i = 1, \dots, 4N\}, & k = 2, \dots, K-1 \\ \text{span}\{\hat{\mathbf{u}}_i, & i = 1, \dots, 2N\}, & k = K \end{cases} \\ \hat{M}_N = M_N(\hat{\Omega}) &= \begin{cases} \text{span}\{\hat{p}_i, & i = N, \dots, 2N+1\}, & k = 1 \\ \text{span}\{\hat{p}_i, & i = 1, \dots, 2N\}, & k = 2, \dots, K-1 \\ \text{span}\{\hat{p}_i, & i = 1, \dots, N\}, & k = K. \end{cases}\end{aligned}\quad (4.2)$$

For the second approach we define

$$\begin{aligned}\hat{X}_N = X_N(\hat{\Omega}) &= \begin{cases} \text{span}\{\hat{\mathbf{u}}_i^{in}, & i = 1, \dots, 2N\}, & k = 1 \\ \text{span}\{\hat{\mathbf{u}}_i^c, & i = 1, \dots, 2N\}, & k = 2, \dots, K-1 \\ \text{span}\{\hat{\mathbf{u}}_i^o, & i = 1, \dots, 2N\}, & k = K \end{cases} \\ \hat{M}_N = M_N(\hat{\Omega}) &= \begin{cases} \text{span}\{\hat{p}_i^{in}, & i = 1, \dots, N\}, & k = 1 \\ \text{span}\{\hat{p}_i^c, & i = 1, \dots, N\}, & k = 2, \dots, K-1 \\ \text{span}\{\hat{p}_i^o, & i = 1, \dots, N\}, & k = K, \end{cases}\end{aligned}\quad (4.3)$$

where superscripts *in*, *c* and *o* indicates whether a basis function represents the inlet subdomain, a central subdomain, or the outflow subdomain. We also recall that the index *k* refers to the subdomain Ω_k . The velocity basis functions are ordered such that the original $N = 15$ have the indices $i = 1, \dots, 15$, and the enriched basis functions corresponding to the original $N = 15$ pressure basis functions have the indices $i = N+1, \dots, 2N$. The reflected original and the reflected enriched basis functions then follow. We remark that the constant pressure basis function added on the inlet domain ($k = 1$) corresponds to the index $i = 2N + 1$, and the associated enriched velocity basis function corresponds to the index $i = 4N + 1$.

On a generic deformed geometry we can then define the reduced basis pressure space as

$$M_N = M_N(\Omega) = \{q \in M, \quad q|_{\Omega_k} \circ \Phi^k \in \hat{M}_N, \quad k = 1, \dots, K\}, \quad (4.4)$$

where Φ^k is the mapping associated with the deformation of the *k*'th subdomain. We also define a preliminary reduced basis velocity space on the deformed geometry as

$$Y_N = Y_N(\Omega) = \{\mathbf{v} \in X, \quad \forall k \exists \hat{\mathbf{v}} \in \hat{X}_N, \quad \mathbf{v}|_{\Omega_k} = \mathcal{I}_N(|J^k|(\mathcal{J}^k)^{-1}(\hat{\mathbf{v}} \circ (\Phi^k)^{-1}) \circ \Phi^k) \circ (\Phi^k)^{-1}\}. \quad (4.5)$$

This space is preliminary since we have not yet imposed any continuity conditions across the subdomain interfaces.

4.2. Matching conditions

As mentioned earlier, we use a mortar element method to glue the velocities together. In practice we try to minimize the jump across internal interfaces by introducing the constraints

$$\int_{\Gamma_{kl}} (\mathbf{v}|_{\Omega_k} - \mathbf{v}|_{\Omega_l}) \cdot \mathbf{n} \psi ds = 0, \quad \forall \psi \in W_{k,l}^n, \quad \forall k, l \quad (4.6)$$

and

$$\int_{\Gamma_{kl}} (\mathbf{v}|_{\Omega_k} - \mathbf{v}|_{\Omega_l}) \cdot \mathbf{t} \psi ds = 0, \quad \forall \psi \in W_{k,l}^t, \quad \forall k, l, \quad (4.7)$$

where $\bar{\Gamma}_{kl} = \bar{\Omega}_k \cap \bar{\Omega}_l$, \mathbf{n} is the unit normal vector of Γ_{kl} , \mathbf{t} is the unit tangential vector, and $W_{k,l}^n$ and $W_{k,l}^t$ are spaces of low order polynomials defined on Γ_{kl} . Depending on the order of the polynomials in $W_{k,l}^n$ and $W_{k,l}^t$, the jump across the interfaces can be controlled; see [14] for results of different polynomial degrees used on a thermal fin problem. Our reduced basis velocity space for Method 1 is then defined as

$$X_N = \{ \mathbf{v} \in Y_N, \quad (4.6) \text{ and } (4.7) \text{ hold} \}. \quad (4.8)$$

For Method 2 we define the reduced basis velocity space as

$$X_N^0 = \{ \mathbf{v} \in X_N, \quad \sum_{k=1}^K \int_{\Omega_k} q \nabla \cdot \mathbf{v} \, d\Omega = 0, \quad \forall q \in M_N \}, \quad (4.9)$$

which is just X_N without the enriched velocity basis functions.

To evaluate the integrals in (4.6) and (4.7), the x - and y -components of \mathbf{v} are rotated to find the corresponding normal and tangential components.

4.3. Numerical results

We define Ω to be the deformed annulus in Figure 2 divided into three subdomains in the flow direction, i.e. $K = 3$. An initial choice of Lagrange multiplier spaces will be

$$W_{k,l}^n = W_{k,l}^t = \mathbb{P}_3(\Gamma_{kl}). \quad (4.10)$$

For Method 1 we solve the problem: Find $\mathbf{u}_N \in X_N$ and $p_N \in M_N$ such that

$$\begin{aligned} a_N(\mathbf{u}_N, \mathbf{w}) + b_N(\mathbf{w}, p_N) &= l_N(\mathbf{w}) \quad \forall \mathbf{w} \in X_N \\ b_N(\mathbf{u}_N, q) &= 0 \quad \forall q \in M_N. \end{aligned} \quad (4.11)$$

In Table 3 we compare the results for the different choices of spaces \hat{X}_N and \hat{M}_N in (4.2) and (4.3).

If we use (4.2) to define \hat{X}_N and \hat{M}_N , the dimension of $X_N \times M_N$ is $12N + 2 - 2L$, where $L = \dim(W_{k,l}^n) + \dim(W_{k,l}^t)$ is the total dimension of the Lagrange multiplier spaces. If we instead use (4.3) to define \hat{X}_N and \hat{M}_N the dimension is only $9N - 2L$, but we still see from Table 3 that the approximation abilities, measured as the norm of the error, are better than the first choice when the dimension of the spaces is comparable. In Figures 6(a) and 6(b), we see that for both choices of reduced basis spaces the error of the pressure is more noticeable close to the internal interfaces relative to the rest of the domain. The velocity error for the first choice of basis spaces, which is shown in Figures 7(a) and 7(b), indicates that the error along the internal interfaces is no larger than in the rest of the domain. The velocity error for the second choice of basis spaces exhibit similar behaviour, which confirms the effect of the weak continuity imposed by the Lagrange multipliers.

In Method 2 we find the reduced basis velocity solution by solving: Find $\mathbf{u}_N \in X_N^0$ such that

$$a_N(\mathbf{u}_N, \mathbf{v}) = l_N(\mathbf{v}) \quad \forall \mathbf{v} \in X_N^0. \quad (4.12)$$

\hat{X}_N, \hat{M}_N	N	$\dim(X_N \times M_N)$	$\ \mathbf{u}_N - \mathbf{u}_N\ _{H^1(\Omega)}$	$\ p_N - p_N\ _{L^2(\Omega)}$
(4.2)	11	118	$1.8 \cdot 10^{-3}$	$9.8 \cdot 10^{-3}$
(4.3)	15	119	$8.4 \cdot 10^{-4}$	$3.6 \cdot 10^{-3}$

TABLE 3. Comparison of the error for different choices of reduced basis spaces in Method 1.

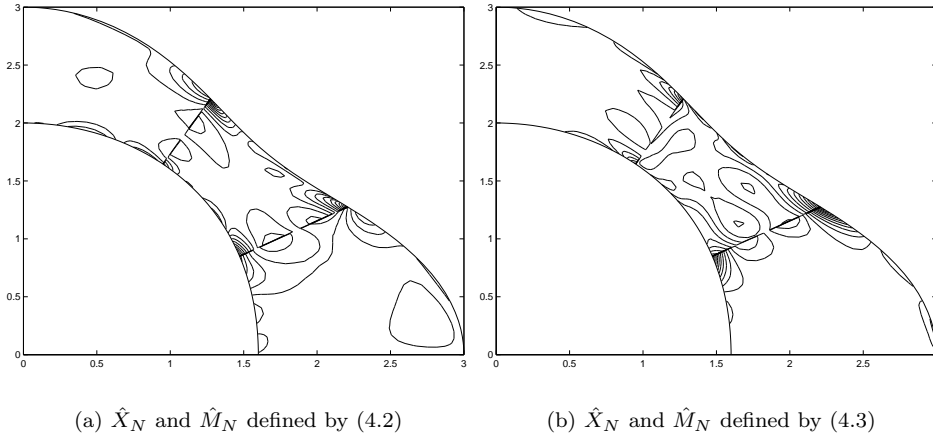


FIGURE 6. Contour of the pressure error for \hat{X}_N and \hat{M}_N defined as in (4.2) and (4.3).

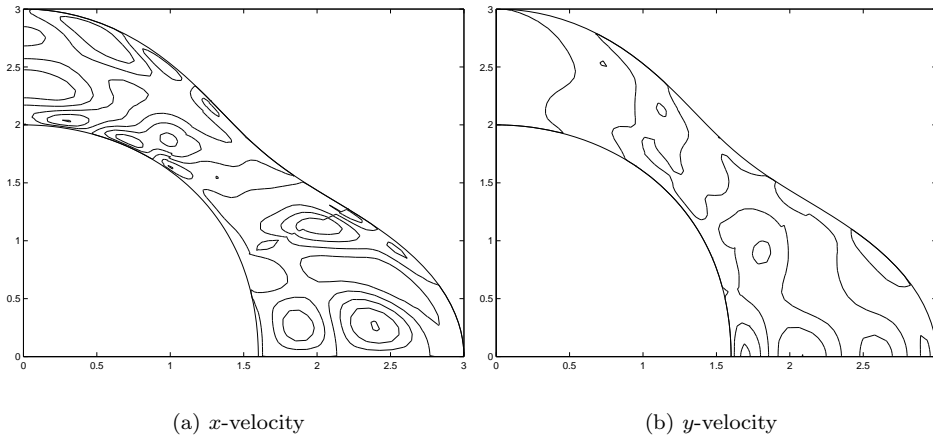


FIGURE 7. Contour of the velocity error for \hat{X}_N and \hat{M}_N defined as in (4.2).

If we use (4.3) to define \hat{X}_N , the dimension of X_N^0 is $3N - 2L$, about one third of the corresponding dimension for Method 1. Having obtained the velocity from (4.12), the pressure is then found by solving the problem: Find $p_N \in M_N$ such that

$$b_N(\mathbf{v}, p_N) = -a_N(\mathbf{u}_N, \mathbf{v}) + l_N(\mathbf{v}) \quad \forall \mathbf{v} \in X_N^e, \quad (4.13)$$

where $X_N^e = \{\mathbf{v} \in X_N, \mathbf{v} \notin X_N^0\}$ contains the enriched velocity basis functions found earlier. On three subdomains we can find the pressure by solving three decoupled systems, each system being of dimension N .

To further study the convergence properties of Method 1 and 2, we use (4.3) for different choices of N to solve (4.11) and (4.12) respectively. In Table 4 we see that the error of the velocity converges well for both methods. As in the single domain case, Method 2 is just as accurate as Method 1. The pressure found in Method 1 also converges well, and if we use (4.13) to find the pressure in Method 2, it will exhibit similar properties.

N	Method 1				Method 2	
	$d(X_N)$	$d(M_N)$	$ \mathbf{u}_N - \mathbf{u}_N _{H^1}$	$\ p_N - p_N\ _{L^2}$	$d(X_N^0)$	$ \mathbf{u}_N - \mathbf{u}_N _{H^1}$
6	20	18	$2.1 \cdot 10^{-2}$	$6.9 \cdot 10^5$	2	$2.5 \cdot 10^{-2}$
7	26	21	$3.7 \cdot 10^{-3}$	$2.2 \cdot 10^4$	5	$5.8 \cdot 10^{-3}$
8	32	24	$2.7 \cdot 10^{-3}$	$5.5 \cdot 10^{-1}$	8	$2.7 \cdot 10^{-3}$
9	38	27	$2.3 \cdot 10^{-3}$	$3.6 \cdot 10^{-1}$	11	$2.3 \cdot 10^{-3}$
10	44	30	$1.3 \cdot 10^{-3}$	$1.3 \cdot 10^{-1}$	14	$1.3 \cdot 10^{-3}$
11	50	33	$1.2 \cdot 10^{-3}$	$5.8 \cdot 10^{-2}$	17	$1.2 \cdot 10^{-3}$
12	56	36	$9.8 \cdot 10^{-4}$	$6.2 \cdot 10^{-3}$	20	$9.8 \cdot 10^{-4}$
13	62	39	$9.7 \cdot 10^{-4}$	$4.4 \cdot 10^{-3}$	23	$9.7 \cdot 10^{-4}$
14	68	42	$8.7 \cdot 10^{-4}$	$4.6 \cdot 10^{-3}$	26	$8.7 \cdot 10^{-4}$
15	74	45	$8.4 \cdot 10^{-4}$	$3.6 \cdot 10^{-3}$	29	$8.4 \cdot 10^{-4}$

TABLE 4. The error convergence of Method 1 and Method 2 in the multi domain case, $d(\cdot)$ is the dimension of the space in question.

4.4. The effect of different Lagrange multipliers

We have already seen that the approximation properties are affected by the choice of basis functions in the reduced basis velocity and pressure spaces. In this section we will try different choices of Lagrange multiplier spaces used in the mortar element method. Previously we used $W_{k,l}^n = W_{k,l}^t = \mathbb{P}_3(\Gamma_{kl})$ to get the results in Tables 3 and 4. However, it is not necessary to use the same space in the normal and tangential direction. Considering the incompressibility condition, the normal derivative is more important than the tangential condition since a good matching of the normal derivative along an interface is directly related to a good mass conservation (or continuity of the volume flow rate across an interface). It would also be advantageous to lower the dimension on the space in the tangential direction compared to the space in the normal direction in order to decrease the number of constraints imposed on the reduced basis system. In the three dimensional case there are two tangential directions and only one normal direction on each interface, and lowering the dimension of the tangential spaces becomes more important. The velocity components are connected through the divergence free property, but a minimization of the jump in the normal velocity component alone across an interface does not guarantee that the tangential velocity component points in the same direction along an interface. To illustrate this we first define

$$\begin{aligned} W_{k,l}^n &= \mathbb{P}_3(\Gamma_{kl}) \\ W_{k,l}^t &= \emptyset, \end{aligned} \tag{4.14}$$

where we have no constraint in the tangential direction, and then

$$\begin{aligned} W_{k,l}^n &= \mathbb{P}_3(\Gamma_{kl}) \\ W_{k,l}^t &= \mathbb{P}_1(\Gamma_{kl}), \end{aligned} \tag{4.15}$$

where we use linear functions in the tangential direction. The results are presented in Table 5 together with the results from the previous choice of $W_{k,l}^n$ and $W_{k,l}^t$.

If we increase the polynomial degree in the Lagrange multiplier spaces, the discontinuities across the interfaces will decrease, but the number of degrees of freedom in the global reduced basis element problem will also decrease and hence the global error may increase. We keep the linear functions in the tangential direction, and calculate

$W_{k,l} = W_{k,l}^n \times W_{k,l}^t$	$\ \mathbf{u}_N - \mathbf{u}_N\ _{H^1}$	$\ p_N - p_N\ _{L^2}$
$\mathbb{P}_3 \times \mathbb{P}_3$	$8.4 \cdot 10^{-4}$	$3.6 \cdot 10^{-3}$
$\mathbb{P}_3 \times \emptyset$	$6.6 \cdot 10^{-2}$	$1.4 \cdot 10^{-1}$
$\mathbb{P}_3 \times \mathbb{P}_1$	$7.2 \cdot 10^{-4}$	$2.1 \cdot 10^{-3}$
$\{\tilde{\psi}_{kl}^i\}$ from (4.18), $i = 1, 2, 3$	$1.5 \cdot 10^{-3}$	$6.7 \cdot 10^{-3}$
$\{\tilde{\psi}_{kl}^i\}$ from (4.18), $i = 2, 4, 6$	$6.8 \cdot 10^{-4}$	$1.3 \cdot 10^{-3}$
$\{\psi_{kl}\}$ from (4.17)	$6.0 \cdot 10^{-4}$	$1.1 \cdot 10^{-3}$

TABLE 5. The norm of the error for different choices of $W_{k,l}^n$ and $W_{k,l}^t$.

the error for different polynomial degrees in the normal direction, i.e.

$$\begin{aligned} W_{k,l}^n &= \mathbb{P}_m(\Gamma_{kl}) \\ W_{k,l}^t &= \mathbb{P}_1(\Gamma_{kl}). \end{aligned} \quad (4.16)$$

From Table 6 we see that the error has a minimum when the polynomial degree m in the normal direction is between two and seven. This is consistent with the results presented in [14] for a scalar heat transfer problem with only one Lagrange multiplier space.

From the consistency error defined in (4.1), we see that the best Lagrange multipliers should be ones that are close to the exact stress vector

$$\boldsymbol{\psi}_{kl} = \left(\nu \frac{\partial \mathbf{u}_N}{\partial \mathbf{n}} - p_N \mathbf{n} \right)_{|\Gamma_{kl}}, \quad (4.17)$$

on each interface Γ_{kl} . We therefore calculate

$$\boldsymbol{\psi}_{kl}^i = \left(\nu \frac{\partial \mathbf{u}_i}{\partial \mathbf{n}_i} - p_i \mathbf{n}_i \right)_{|\Gamma_{kl}^i}, \quad (4.18)$$

for all Ω_i . Similar to the velocity basis functions, \mathbf{u}_i , the stress vectors are mapped to a reference interface $\hat{\Gamma}$ through the Piola transformation, $\hat{\boldsymbol{\psi}}_{kl}^i = \Psi_i(\boldsymbol{\psi}_{kl}^i)$. On the generic domain Ω we first map each $\hat{\boldsymbol{\psi}}_{kl}^i$ to corresponding interfaces Γ_{kl} , again using the Piola transformation $\tilde{\boldsymbol{\psi}}_{kl}^i = \Psi^{-1}(\hat{\boldsymbol{\psi}}_{kl}^i)$, and then rotate the coordinates to find the normal and tangential components. The space $W_{k,l}^n$ will thus consist of the normal components of

m	$\ \mathbf{u}_N - \mathbf{u}_N\ _{H^1}$	$\ p_N - p_N\ _{L^2}$
1	$4.94 \cdot 10^{-3}$	$4.66 \cdot 10^{-3}$
2	$8.22 \cdot 10^{-4}$	$2.24 \cdot 10^{-3}$
3	$7.17 \cdot 10^{-4}$	$2.06 \cdot 10^{-3}$
4	$7.17 \cdot 10^{-4}$	$2.07 \cdot 10^{-3}$
5	$6.91 \cdot 10^{-4}$	$2.00 \cdot 10^{-3}$
6	$6.93 \cdot 10^{-4}$	$2.00 \cdot 10^{-3}$
7	$7.00 \cdot 10^{-4}$	$2.17 \cdot 10^{-3}$
8	$7.15 \cdot 10^{-4}$	$2.24 \cdot 10^{-3}$
9	$8.25 \cdot 10^{-4}$	$2.74 \cdot 10^{-3}$

TABLE 6. The norm of the error when $W_{k,l}^t$ and $W_{k,l}^n$ are defined as in (4.16).

the $\tilde{\psi}_{kl}^i$, and $W_{k,l}^t$ of the tangential components. We impose (4.6) and (4.7), which in turn ensures that the vectorial jump

$$\sum_{k,l} \int_{\Gamma_{kl}} (\mathbf{u}_{N|\Omega_k} - \mathbf{u}_{N|\Omega_l}) \cdot \tilde{\psi}_{kl}^i ds = 0, \quad \forall i. \quad (4.19)$$

In order to balance the number of constraints against the number of degrees of freedom, we choose the same number of constraints as for the $\mathbb{P}_3 \times \mathbb{P}_1$ case, but now with $\dim(W_{k,l}^n) = \dim(W_{k,l}^t) = 3$; the total number of constraints is thus six. Depending on which three multipliers are used, we get different results. The worst result is achieved for $i = 1, 2$ and 3 , while the best result is achieved for $i = 2, 4$ and 6 ; see Table 5. Compared to the Lagrange multiplier spaces defined as low order polynomials, we see that the stress vectors (4.18) give better results, however, care has to be taken as to which three stress vectors are used. As a final test, we use the exact stress vector (4.17) to produce a single constraint in each of the spatial directions. This should give zero consistency error and result in a pure approximation error in the reduced basis element solution. As expected, the numerical result is also better than for all other Lagrange multipliers; see Table 5.

5. CONCLUSIONS

In this paper, we have proposed a reduced basis element method for the steady Stokes problem. The computational method is based on a domain decomposition into geometrically similar parts (denoted as “elements”), and local approximations based on precomputed steady Stokes solutions corresponding to different geometric shapes (denoted as geometric “snapshots”). The proposed method represents an extension of earlier work associated with solving the Laplace equation.

The precomputed velocity fields are (weakly) incompressible on the preselected geometries. We have used Piola’s transformation to ensure that this property is also satisfied on the reference domain associated with the computational parts, and also when mapped to a new and unknown geometric shape. The issue of satisfying the inf-sup condition has been addressed in two different ways.

One alternative, called Method 1, is based on enriching the reduced velocity basis in order to obtain a stable, coupled system for the velocity and the pressure. A second alternative, called Method 2, directly exploits the fact that the precomputed velocity fields are almost incompressible. Following this latter method, the Stokes system is reduced to solving a Poisson-like equation for the velocity. The pressure can then be computed in a postprocessing step. The advantages of this alternative are the facts that the velocity and the pressure can be computed separately, and very small systems need to be solved.

We have demonstrated the approximation and convergence properties of Method 1 and Method 2 on selected two-dimensional problems. The numerical results are almost identical, suggesting that Method 2 is very attractive due to the lower computational cost.

The methods have been tested both in the single-domain context and using multiple subdomains. In the latter case, the local velocity approximations are glued together using the mortar element method. Proper treatment of the continuity conditions for the normal and tangential velocity components is discussed. It has been found that it is sufficient to use a very low dimension of the Lagrange multiplier space associated with the tangential component.

In the single-domain context we have also developed *a posteriori* error estimators for the steady Stokes problem and the theoretical results have been confirmed by numerical experiments in the compliant case. For the particular test problem used, the lower bound gap appears to be very good, while the upper bound gap is somewhat conservative.

Future extensions will include the simulation of geometrically more complex systems involving several types of computational parts (e.g., pipes and bifurcations). In addition, it will be interesting to exploit the properties of Method 2 to solve unsteady problems, including problems modeled by the incompressible Navier-Stokes equations. Finally, the *a posteriori* error estimators developed here need to be extended to the general non-compliant multiple element case, as was done in [14].

This work has been supported by the Research Council of Norway through the BeMatA programme under contract 147044/431, by the RTN project HaeMOdel HPRN-CT-2002-00270, and the ACI project "le-poumon-vous-dis-je" granted by the Fond National pour la Science. The support is gratefully acknowledged.

REFERENCES

- [1] R. Aris. *Vectors, Tensors and the Basic Equations of Fluid Mechanics*. Dover Publications, 1989.
- [2] I. Babuska. Error-bounds for finite element method. *Numer. Math.*, 16:322–333, 1971.
- [3] B. F. Belgacem. The mortar finite element method with Lagrange multipliers. *Numer. Math.*, pages 173–197, 1999.
- [4] B. F. Belgacem, C. Bernardi, N. Chorfi, and Y. Maday. Inf-sup conditions for the mortar spectral element discretization of the Stokes problem. *Numer. Math.*, 85:257–281, 2000.
- [5] C. Bernardi and Y. Maday. Polynomial approximation of some singular functions. *Appl. Anal.*, 42:1–32, 1992.
- [6] F. Brezzi. On the existence, uniqueness and approximation of saddle-point problems arising from Lagrange multipliers. *Rairo Anal. Numer.*, 8 R2:129–151, 1974.
- [7] F. Brezzi and M. Fortin. *Mixed and Hybrid Finite Element Methods*. Springer Verlag, 1991.
- [8] J. P. Fink and W. C. Rheinboldt. On the error behavior of the reduced basis technique in nonlinear finite element approximations. *Z. Angew. Math. Mech.*, 63:21–28, 1983.
- [9] W. J. Gordon and C. A. Hall. Construction of curvilinear co-ordinate systems and applications to mesh generation. *Int J. Numer. Methods Eng.*, 7:461–477, 1973.
- [10] Y. Maday, D. Meiron, A. T. Patera, and E. M. Rønquist. Analysis of iterative methods for the steady and unsteady Stokes problem: Application to spectral element discretizations. *SIAM J. Sci. Stat. Comp.*, pages 310–337, 1993.
- [11] Y. Maday and A. T. Patera. Spectral element methods for the Navier-Stokes equations. In Noor A. (ed) *State of the Art Surveys in Computational Mechanics*, pages 71–143, 1989.
- [12] Y. Maday, A. T. Patera, and E. M. Rønquist. The $P_N \times P_{N-2}$ method for the approximation of the Stokes problem. *Technical Report No. 92009, Department of Mechanical Engineering, Massachusetts Institute of Technology*, 1992.
- [13] Y. Maday and E. M. Rønquist. A reduced-basis element method. *J. Sci. Comput.*, 17:447–459, 2002.
- [14] Y. Maday and E. M. Rønquist. The reduced-basis element method: Application to a thermal fin problem. *SIAM J. Sci. Comput.*, 26(1):240–258, 2004.
- [15] A. K. Noor and J. M. Peters. Reduced basis technique for nonlinear analysis of structures. *AIAA J.*, 18(4):455–462, 1980.
- [16] C. Prud'homme, D. V. Rovas, K. Veroy, L. Machiels, Y. Maday, A. T. Patera, and G. Turinici. Reliable real-time solution of parametrized partial differential equations: Reduced basis output bound methods. *J. Fluids Engineering*, 124:70–80, 2002.
- [17] P. A. Raviart and J. M. Thomas. A mixed finite element method for 2-nd order elliptic problems. In I. Galligani and E. Magenes, editors, *Mathematical Aspects of Finite Element Methods, Lecture Notes in Mathematics, Vol. 606*. Springer-Verlag, 1977.
- [18] D. V. Rovas. *Reduced-Basis Output Bound Methods for Parametrized Partial Differential Equations*. PhD thesis, Massachusetts Institute of Technology, Cambridge, MA, October 2002.
- [19] K. Veroy, C. Prud'homme, D. V. Rovas, and A. T. Patera. *A Posteriori* error bounds for reduced-basis approximation of parametrized noncoercive and nonlinear elliptic partial differential equations (AIAA Paper 2003-3847). In *Proceedings of the 16th AIAA Computational Fluid Dynamics Conference*, June 2003.